REPORT

MOLECULAR BIOLOGY

Human cohesin compacts DNA by loop extrusion

Yoori Kim[1]*, Zhubing Shi[1]*, Hongshan Zhang[2], Ilya J. Finkelstein[2]†, Hongtao Yu[1]†

Cohesin is a chromosome-bound, multisubunit adenosine triphosphatase complex. After loading onto chromosomes, it generates loops to regulate chromosome functions. It has been suggested that cohesin organizes the genome through loop extrusion, but direct evidence is lacking. Here, we used single-molecule imaging to show that the recombinant human cohesin-NIPBL complex compacts both naked and nucleosome-bound DNA by extruding DNA loops. DNA compaction by cohesin requires adenosine triphosphate (ATP) hydrolysis and is force sensitive. This compaction is processive over tens of kilobases at an average rate of 0.5 kilobases per second. Compaction of double-tethered DNA suggests that a cohesin dimer extrudes DNA loops bidirectionally. Our results establish cohesin-NIPBL as an ATP-driven molecular machine capable of loop extrusion.

The ring-shaped cohesin complex binds chromosomes both topologically and nontopologically and regulates diverse chromosome-based processes, including chromosome segregation, DNA repair, and transcription (1–7). Human cohesin consists of the SMC1-SMC3 heterodimeric adenosine triphosphatase (ATPase), the kleisin subunit RAD21 that links the ATPase heads, and either of the helical repeat proteins STAG1 or STAG2 (Fig. 1A). Cohesin is loaded on chromosomes by the NIPBL-MAU2 complex (8–10). Mutations of cohesin subunits and NIPBL result in human developmental diseases with multisystem dysfunctions, collectively referred to as cohesinopathy (9, 11), likely because of transcriptional defects caused by cohesin deficiency. High-throughput chromosome conformation capture (Hi-C) experiments suggest that cohesin mediates the formation of chromosome loops and topologically associated domains (TADs) through a process called loop extrusion (5, 12–20). Single-molecule studies have demonstrated that the related SMC complex condensin can extrude DNA loops (21, 22). By contrast, cohesin has been reported to slide on DNA through adenosine triphosphate (ATP)–independent passive diffusion in vitro (23–25). Whether cohesin also has intrinsic loop extrusion activity remains an open question. Here, we addressed this question with single-molecule studies using recombinant human cohesin.

The cohesin loader NIPBL remains bound to cohesin on chromosomes (26, 27) and is required for chromosome looping in cells (15).

We thus expressed and purified the recombinant human cohesin complex alone or bound to the C-terminal region of NIPBL (NIPBL[C], residues 1163 to 2804) in insect cells (Fig. 1B and fig. S1A). Cohesin alone had low basal ATPase activity, and this activity was greatly stimulated by NIPBL[C] and DNA (Fig. 1C) (28, 29). The ATPase-deficient cohesin SMC1A-E1157Q/SMC3-E1144Q (EQ) mutant exhibited minimal ATPase activity even in the presence of NIPBL[C] and DNA. Negative-stain electron microscopy showed that 51% (n = 352) of the chemically cross-linked cohesin-NIPBL[C] complex particles displayed a bent-rod-like conformation with an overall length of ~50 nm (fig. S1, B and C), whereas the rest of the particles had a shorter, thicker rod shape with a length of ~33 nm. These conformations likely represent different forms of cohesin, with SMC1-SMC3 hinge domains partially or fully folded back toward their head domains, as had been previously observed for both human and yeast cohesin (30, 31).

If cohesin can extrude DNA loops, then it would be expected to compact DNA. To test this possibility, we used total internal reflection fluorescence microscopy to observe aligned arrays of DNA molecules on a lipid bilayer surface in real time (Fig. 1D and movie S1) (32, 33). DNA was stained with the green fluorescent dye YOYO-1. After incubating the DNA curtains with unlabeled cohesin-NIPBL[C] in the absence of buffer flow, we observed that all DNA molecules were completely compacted to the barrier in the presence of ATP (fig. S2), and this compaction could not be reversed by resuming flow.

We then fluorescently labeled NIPBL[C] with quantum dots (QDs) to visualize the cohesin-NIPBL[C] complex. The QD-labeled cohesin-NIPBL[C] complexes rapidly bound to the DNA array as soon as it entered the flow cell (Fig. 1E). We observed single QD-tagged complexes, as indicated by intermittent QD photoblinking

(34), but could not completely rule out QD-tagged cohesin oligomers (see below). Analysis of the initial binding distribution of the cohesin-NIPBL[C] complexes on the DNA substrate showed preferential loading on AT-rich regions (fig. S3, A and B), which was also observed for cohesin alone and for condensin (21, 24). We also measured the one-dimensional diffusion activity of the cohesin-NIPBL[C] complex on double-tethered DNA curtains (fig. S3, C and D). The complex was stably bound on DNA for >5 min and diffused slowly in an ATP-independent manner, with an average diffusion coefficient of $0.02 \pm 0.003\ \mu m^2\ s^{-1}$ (mean ± SEM; fig. S3, E and F), which is eightfold lower than that reported for human cohesin topologically bound to DNA (25). Thus, the cohesin-NIPBL[C] complex displays very limited diffusion activity on DNA.

After the initial binding of cohesin-NIPBL[C] complexes to single-tethered DNA, we observed time-dependent, gradual DNA compaction (Fig. 1F and movie S2). We then measured the extent and rate of cohesin-mediated DNA compaction at different applied forces (i.e., flow rates; Fig. 1, F to H) (35). At an initial applied force of 0.3 pN, the DNA was almost completely compacted, with an average rate of 0.5 kb s^{-1}. When the initial applied force increased to 0.6 pN, we detected incomplete DNA condensation with a correspondingly slower compaction rate. There was minimal DNA compaction by cohesin-NIPBL[C] at 0.8 pN of applied force. Although the applied force changes for DNA molecules as they begin compacting, the force-sensitive cohesin translocation is qualitatively similar to condensin-mediated DNA looping (22). Reducing the salt concentration from 50 to 25 mM increased the extent and rate of DNA compaction by cohesin at high flow rates (fig. S4), suggesting that stronger cohesin-DNA or cohesin-cohesin interactions (as can occur in a crowded nuclear milieu) can raise the force threshold of compaction.

Cohesin alone (without NIPBL[C]) with its RAD21 subunit labeled with QDs did not bind or compact DNA even in the presence of ATP (fig. S5A), indicating a requirement for NIPBL in loading cohesin onto DNA. The slowly hydrolyzable ATP analog adenylyl-imidodiphosphate (AMP-PNP) could not support efficient DNA compaction (fig. S5, A and B). The ATPase-deficient cohesin EQ mutant, which was expected to retain nucleotide-binding activity, was also deficient in DNA compaction even in the presence of NIPBL[C] and ATP. Thus, cohesin-NIPBL[C]-dependent DNA compaction requires ATP hydrolysis.

We never detected stepwise DNA condensation events, suggesting that DNA compaction by cohesin-NIPBL[C] is not mediated through search and capture of distant DNA segments. Instead, we observed frequent cohesin-NIPBL[C] slippage events at 0.3 pN of applied force

[1]Department of Pharmacology, University of Texas Southwestern Medical Center, Dallas, TX 75390, USA. [2]Center for Systems and Synthetic Biology, Institute for Cellular and Molecular Biology, Department of Molecular Biosciences, University of Texas at Austin, Austin, TX 78712, USA.
*These authors contributed equally to this work.
†Corresponding author. Email: ilya@finkelsteinlab.org (I.J.F.); hongtao.yu@utsouthwestern.edu (H.Y.)

Fig. 1. Human cohesin-NIPBL^C compacts linear DNA. (**A**) Schematic representation of human cohesin-NIPBL. CC, coiled coil. (**B**) Coomassie staining of purified recombinant human cohesin and cohesin-NIPBL^C. WT, wild type. (**C**) ATPase activities (mean ± SEM) of human cohesin and cohesin-NIPBL^C (50 nM) in the absence or presence of 500 nM 40-bp double-stranded DNA (dsDNA). (**D**) Illustration of DNA curtains bound by human cohesin-NIPBL^C. One end of DNA is tethered to the surface. (**E**) Image of fluorescently labeled cohesin-NIPBL^C (magenta) on single-tethered DNA molecules stained with YOYO-1 (green). (**F**) Representative kymographs showing DNA condensation mediated by cohesin-NIPBL^C at two applied forces. Red gradient triangle indicates the protein injection time window. The concentration of protein traversing the flow cell was diluted for a few minutes by constant buffer flow. (**G** and **H**) Quantification of the percentage of DNA length condensed (G) and the DNA condensation rate (H). Boxplots indicate the median, 10th, and 90th percentiles of the distribution. p-values are obtained from two-tailed t test: ****$p < 0.0001$. At least 25 DNA molecules were measured for each condition.
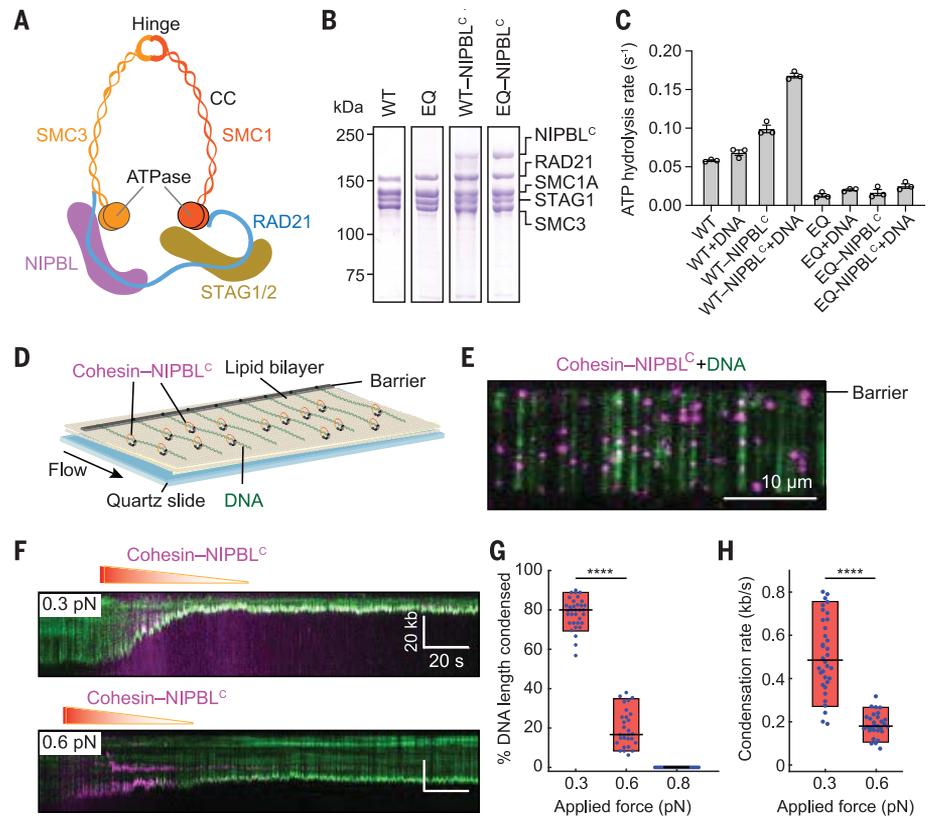
Fig. 2. Cohesin-NIPBL^C compacts nucleosomal DNA.
(**A**) Illustration of nucleosomal DNA compaction by cohesin-NIPBL^C. (**B**) Image of QD-labeled nucleosomes deposited on single-tethered DNA curtain with or without flow. (**C**) Distribution of the number of nucleosomes per DNA (mean ± SD). (**D**) Representative kymographs of the compaction of nucleosome-bound DNA by WT or EQ cohesin-NIPBL^C at different applied forces with or without ATP. (**E**) Percentage of the length of nucleosome-bound DNA condensed in (D). (**F**) Compaction rate of nucleosome-bound DNA by cohesin-NIPBL^C. At least 25 DNA molecules were measured for each condition in (E) and (F).
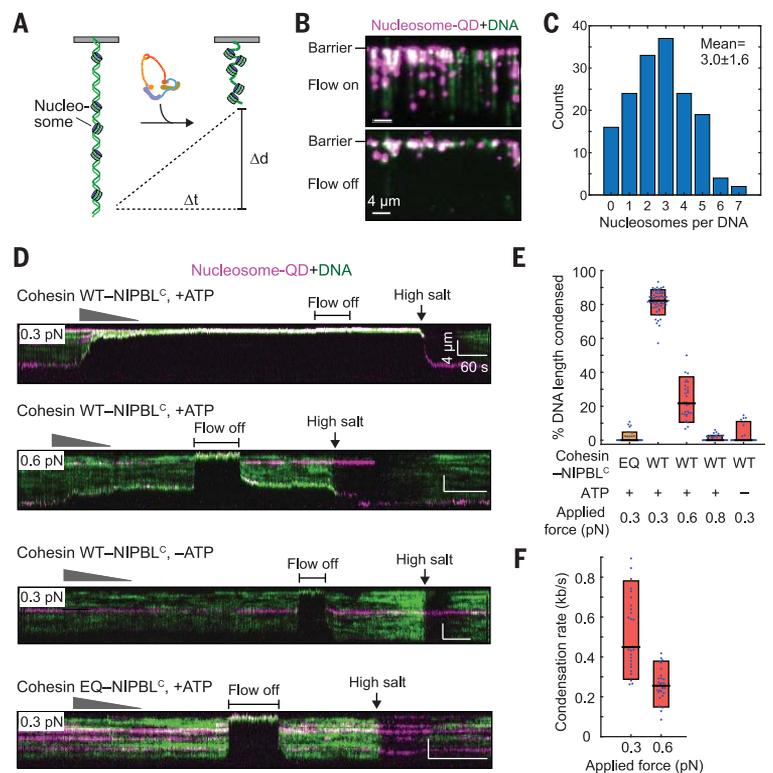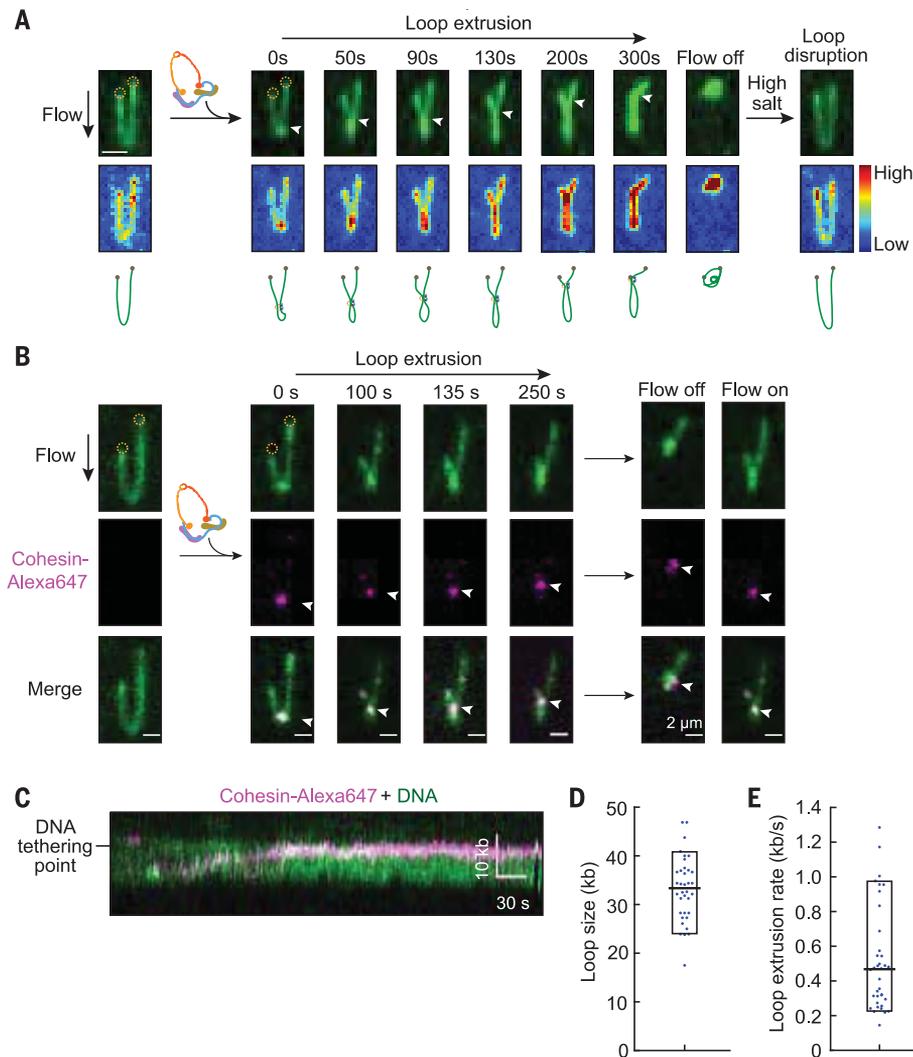
Fig. 3. Real-time visualization of loop extrusion by cohesin-NIPBL[C]. (**A**) Time course showing DNA loop extrusion by cohesin-NIPBL[C] on YOYO-1–stained U-shaped DNA (top). Scale bar, 2 μm. Both DNA ends (dashed circle) are tethered to the surface and the extruding loop is extended at 0.1 ml/min buffer flow. Upon cohesin-NIPBL[C] injection, a small loop appeared at the tip of the DNA and elongated until the base of the loop (arrow) reached one tethering point. A brief shutoff of flow retracted DNA completely, indicating that DNA was not stuck to the surface. Injection of a high-salt buffer (500 mM NaCl) disrupted the loop. The scaled color map (middle panel) shows that the DNA intensity matches the growing loop. The schematic drawing (bottom panel) depicts a model of loop extrusion. (**B**) Time-course montage of loop extrusion showing the localization of labeled cohesin-NIPBL[C] (indicated by white arrowheads) at the base of the DNA loop. Turning the flow on and off showed that the cohesin-NIPBL[C] complex moved with the DNA, confirming that it was indeed bound to the DNA loop. (**C**) Representative kymograph showing the movement of a labeled cohesin-NIPBL[C] complex toward the DNA-tethering points. (**D** and **E**) Quantification of the loop size (D) and the rate of loop extrusion (E) by Alexa647-labeled cohesin-NIPBL[C].

(fig. S6). These observations suggested that cohesin can slide backward on DNA. The rate of the backtracking was similar to that of compaction (fig. S6C). The gradual, processive, ATP-dependent DNA compaction by cohesin-NIPBL[C] with occasional slippage indicated that cohesin is a bona fide molecular motor.

After DNA was fully compacted by cohesin-NIPBL[C] at 0.3 pN, increasing the applied force to 0.8 pN did not fully extend the DNA, and the bound cohesin only backtracked slightly (fig. S6A). This suggested that the completion of DNA compaction might lead to the formation of more stable cohesin-DNA assemblies, providing a plausible explanation for the observation that ATP is not required to maintain cohesin-dependent TADs after their formation in cells (18).

Cohesin can bind DNA by entrapment of DNA inside the lumen of its ring (topological binding) or by physical interaction with DNA that does not involve the opening of its ring (nontopological binding). Topological DNA binding is salt resistant (29). Injection of high-salt buffer dislodged the bound cohesin and fully reversed DNA compaction (fig. S6A and movie S3). Thus, cohesin-NIPBL[C] that is capable of loop extrusion might not be topologically bound to DNA. Analysis of the fluorescent intensities from DNA and QD-protein complexes indicated that cohesin-mediated DNA compaction preferably occurred at the untethered DNA ends (figs. S6A and S7). The underlying reason for this preference is unclear but could be due to the ease of formation of seed DNA loops near the ends or flow-induced higher occupancy of cohesin at DNA ends. Regardless, our data indicated that cohesin-NIPBL[C] is a processive DNA motor that compacts DNA.

DNA is packaged into chromatin in the nucleus. We next tested whether cohesin-NIPBL[C] could compact nucleosome-bound DNA (Fig. 2A). We incorporated one to six QD-labeled human nucleosomes on each DNA substrate using salt dialysis (Fig. 2, B and C) and visualized the nucleosome-bound DNA substrate upon injection of unlabeled cohesin-NIPBL[C] at multiple applied forces (Fig. 2D). The extent of nucleosome-

DNA compaction was ~80% (Fig. 2E) and the average rate of the compaction was 0.5 kb s^{-1} (Fig. 2F). Compaction of nucleosome-bound DNA was also force sensitive and dependent on ATP hydrolysis (Fig. 2, D to F). Thus, cohesin-NIPBL[C] compacts nucleosome-bound DNA with properties similar to those of naked DNA. Nucleosomes impede the movement of topologically loaded cohesin (23, 24). Our finding that cohesin-NIPBL[C] compacts naked and nucleosome-bound DNA with similar rates again suggested that the loop-extruding cohesin might not be topologically loaded. Furthermore, high-salt washout of cohesin revealed that nucleosomes themselves were not repositioned during cohesin-dependent compaction (Fig. 2D). These data suggested that cohesin can act on chromatin without having to displace or slide nucleosomes.

To directly visualize loop extrusion by cohesin, we prepared U-shaped DNA by tethering both DNA ends to the surface and monitored the looping events in real time (movie S4). A small loop formed immediately after cohesin-NIPBL[C]

Fig. 4. Cohesin-NIPBL^C dimers promote loop extrusion. (**A**) Top panel: Representative image of Alexa647-labeled cohesin-NIPBL^C complexes bound to both the base and the tip of a DNA loop. Bottom panel: Number of Alexa647-cohesin foci on each DNA loop (n = 51 DNA molecules). Scale bar, 2 μm. (**B**) Representative two-step photobleaching trace of cohesin at the loop base plotted with the corresponding DNA loop image and its kymograph shown above the trace. Dashed red lines are the photobleaching steps; gray shading is intermittent blinking indicating single fluors. a.u., arbitrary units. (**C**) Intensity distribution of single photobleaching steps of Alexa647-cohesin at the DNA loop fit to a Gaussian distribution (red line). (**D**) Distribution of the number of cohesin-NIPBL^C molecules at the DNA loop base (left panel) and at the loop tip (right panel). (**E**) Model for bidirectional loop extrusion by a cohesin-NIPBL^C dimer.
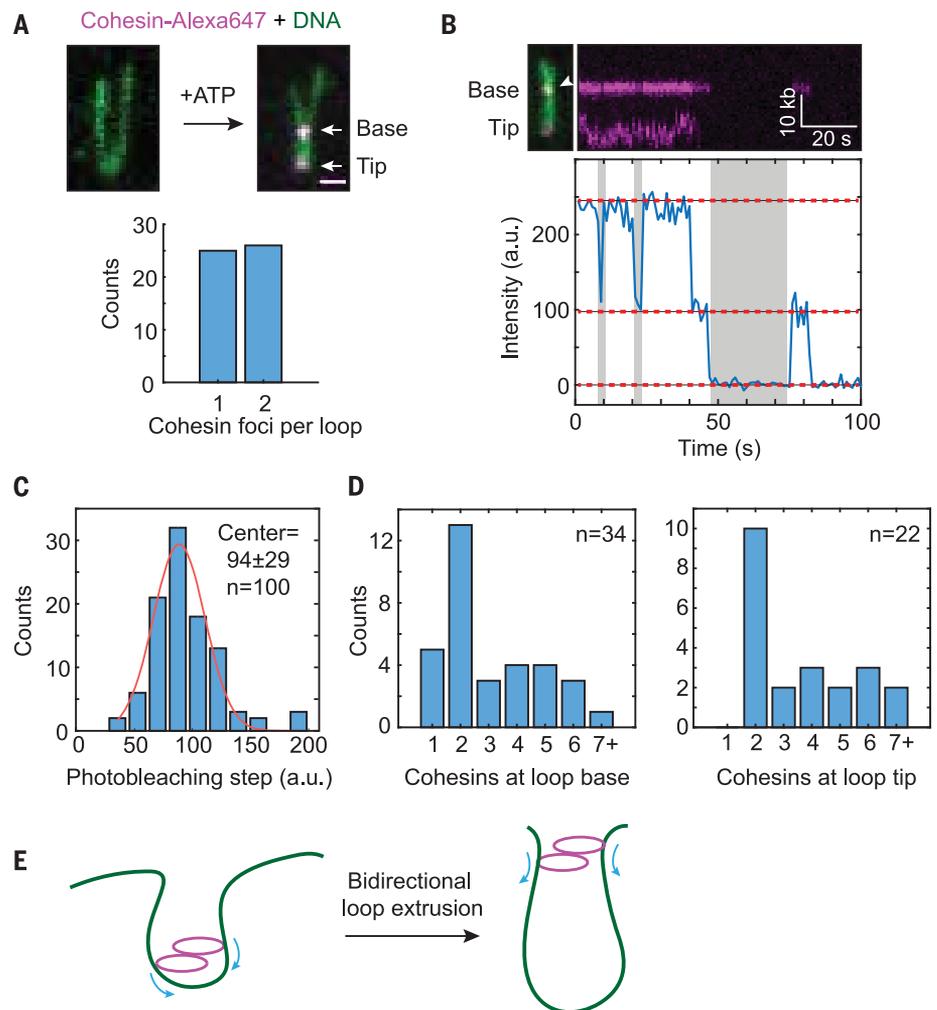
injection and gradually elongated until the motor stalled or one side of the loop reached either DNA-tethering point (Fig. 3A, fig. S8A, and movies S5 to S7). Both arms of the U-shaped DNA were shortened during the process. These results are consistent with cohesin-NIPBL^C extruding DNA loops bidirectionally, as unidirectional asymmetric loop extrusion is expected to shorten only one arm of the U-shaped DNA. The loop was stably maintained for a few minutes, and injection of a high-salt buffer quickly restored the DNA to its original U shape (movie S8). As expected, we did not detect any looping activity in the absence of ATP or with the cohesin EQ mutant.

To visualize cohesin-NIPBL^C at the base of the loop, we directly labeled cohesin-NIPBL^C containing SNAP$_f$-tagged STAG1 with Alexa Fluor 647 dye (Alexa647). Alexa647-labeled cohesin completely compacted DNA with a similar rate as the unlabeled complex (fig. S8B). Cohesin-NIPBL^C bound at the base of the extruding loop (Fig. 3B, fig. S8C, and movie S9). Consistent with symmetric, bidirectional loop extrusion, cohesin-NIPBL^C moved toward DNA-tethering points during the process (Fig. 3C).

The average size of extruded loops was 33 kb and the mean rate of loop extrusion was 0.5 kb s^{-1} (Fig. 3, D and E).

A single condensin complex can extrude DNA loops asymmetrically and in one direction (*22*). A single cohesin complex might be able to perform symmetric loop extrusion. Alternatively, two cohesin complexes might act in concert to extrude loops in both directions. To determine how many cohesin molecules perform loop extrusion, we analyzed photobleaching steps of Alexa647-labeled cohesin-NIPBL^C on DNA loops. On ~50% of DNA loops, we observed two fluorescent foci, with one each at the loop base and tip (Fig. 4A). The number of photobleaching steps of both Alexa647-cohesin foci peaked at two (Fig. 4, B to D). Cohesin foci on DNA that did not form loops had no discrete peaks for the number of photobleaching steps. Thus, the loop-extruding complexes most frequently contained two cohesin molecules. These data suggested that a cohesin-NIPBL^C dimer might be the minimal functional unit for loop extrusion.

Collectively, our results support a model in which a cohesin-NIPBL^C dimer extrudes DNA loops symmetrically in both directions (Fig. 4E). Bidirectional loop extrusion by a cohesin dimer also explains the observed and simulated Hi-C maps of chromosome loops (*5, 19*). We observed loop extrusion by recombinant human cohesin-NIPBL^C at relatively low applied forces and low salt concentrations. We anticipate that cellular crowding, MAU2, the N-terminal region of NIPBL, and other cohesin interactors further stabilize cohesin on DNA and enhance its intrinsic loop extrusion activity in cells.

High-salt buffer dislodged loop-extruding cohesin from DNA. Cohesin-NIPBL^C bound to DNA at low salt exhibited diffusion kinetics much slower than those of topologically loaded cohesin. Finally, nucleosomes do not hinder cohesin-mediated DNA compaction. These findings suggest that cohesin mediates loop extrusion through nontopological or pseudo-topological interactions with DNA.

REFERENCES AND NOTES

1. J. H. Haarhuis, A. M. Elbatsh, B. D. Rowland, *Dev. Cell* **31**, 7–18 (2014).
2. C. Morales, A. Losada, *Curr. Opin. Cell Biol.* **52**, 51–57 (2018).

3. F. Uhlmann, *Nat. Rev. Mol. Cell Biol.* **17**, 399–412 (2016).
4. G. Zheng, H. Yu, *Sci. China Life Sci.* **58**, 1089–1098 (2015).
5. Á. Sedeño Cacciatore, B. D. Rowland, *Curr. Opin. Genet. Dev.* **55**, 11–18 (2019).
6. J. M. Peters, A. Tedeschi, J. Schmitz, *Genes Dev.* **22**, 3089–3114 (2008).
7. K. Nasmyth, C. H. Haering, *Annu. Rev. Genet.* **43**, 525–558 (2009).
8. R. Ciosk et al., *Mol. Cell* **5**, 243–254 (2000).
9. E. T. Tonkin, T. J. Wang, S. Lisgo, M. J. Bamshad, T. Strachan, *Nat. Genet.* **36**, 636–641 (2004).
10. E. Watrin et al., *Curr. Biol.* **16**, 863–874 (2006).
11. T. Bose, J. L. Gerton, *J. Cell Biol.* **189**, 201–210 (2010).
12. K. Nasmyth, *Annu. Rev. Genet.* **35**, 673–745 (2001).
13. E. Alipour, J. F. Marko, *Nucleic Acids Res.* **40**, 11202–11212 (2012).
14. J. Gassler et al., *EMBO J.* **36**, 3600–3618 (2017).
15. J. H. I. Haarhuis et al., *Cell* **169**, 693–707.e14 (2017).
16. S. S. P. Rao et al., *Cell* **171**, 305–320.e24 (2017).
17. G. Wutz et al., *EMBO J.* **36**, 3573–3599 (2017).
18. L. Vian et al., *Cell* **173**, 1165–1178.e20 (2018).
19. G. Fudenberg et al., *Cell Rep.* **15**, 2038–2049 (2016).
20. A. Tedeschi et al., *Nature* **501**, 564–568 (2013).
21. T. Terakawa et al., *Science* **358**, 672–676 (2017).
22. M. Ganji et al., *Science* **360**, 102–105 (2018).
23. I. F. Davidson et al., *EMBO J.* **35**, 2671–2685 (2016).
24. J. Stigler, G. O. Çamdere, D. E. Koshland, E. C. Greene, *Cell Rep.* **15**, 988–998 (2016).
25. M. Kanke, E. Tahara, P. J. Huis In't Veld, T. Nishiyama, *EMBO J.* **35**, 2686–2698 (2016).
26. J. Rhodes, D. Mazza, K. Nasmyth, S. Uphoff, *eLife* **6**, e30000 (2017).
27. G. Zheng, M. Kanchwala, C. Xing, H. Yu, *eLife* **7**, e33920 (2018).
28. N. J. Petela et al., *Mol. Cell* **70**, 1134–1148.e7 (2018).
29. Y. Murayama, F. Uhlmann, *Nature* **505**, 367–371 (2014).
30. M. T. Hons et al., *Nat. Commun.* **7**, 12523 (2016).
31. F. Bürmann et al., *Nat. Struct. Mol. Biol.* **26**, 227–236 (2019).
32. I. F. Gallardo et al., *Langmuir* **31**, 10310–10317 (2015).
33. M. M. Soniat et al., *Methods Enzymol.* **592**, 259–281 (2017).
34. M. Kuno, D. P. Fromm, H. F. Hamann, A. Gallagher, D. J. Nesbitt, *J. Chem. Phys.* **112**, 3117–3120 (2000).
35. J. M. Schaub, H. Zhang, M. M. Soniat, I. J. Finkelstein, *Langmuir* **34**, 14882–14890 (2018).

ACKNOWLEDGMENTS

SUPPLEMENTARY MATERIALS

Science

Human cohesin compacts DNA by loop extrusion

Yoori KimZhubing ShiHongshan ZhangIlya J. FinkelsteinHongtao Yu

Cohesin extrudes DNA loops

DNA is folded into loops in eukaryotic cells by a process that depends on a ring-shaped adenosine triphosphatase complex called cohesin. Davidson *et al.* and Kim *et al.* now show that in the presence of the NIPBLMAU2 protein complex, the human cohesin complex can function as a molecular motor that extrudes DNA loops with high speed in vitro. In contrast to how it mediates sister chromatid cohesion, cohesin does not appear to entrap DNA topologically during loop extrusion. The results provide direct evidence for the loop extrusion model of chromatin organization and suggest that genome architecture is highly dynamic.

Science, this issue p. 1338, p. 1345

View the article online
https://www.science.org/doi/10.1126/science.aaz4475
Permissions
https://www.science.org/help/reprints-and-permissions

Use of think article is subject to the Terms of service